THE BELL SYSTEM TECHNICAL JOURNAL
Vol. 51, No. 3, March, 1972
Printed in U.S.A.

Computer Modeling of Charge-Coupled Device Characteristics

By G. F. AMELIO

(Manuscript received August 16, 1971)

Properties of various charge-coupled device (CCD) configurations are investigated by means of a computer model. The model is based on a numerical solution of the Poisson equation for a unit cell of the CCD structure. The surface potential and the tangential surface electric field are obtained to an estimated accuracy of one percent and used to calculate transfer characteristics. On this basis various devices are compared as a function of both geometrical and electrical parameters. The geometrical parameters include oxide thickness, gap length, and electrode length. The electrical parameters include such things as doping density, fixed interface charge, and applied voltage. The influence of surface states is omitted from the treatment.

The principal results indicate that (i) for dimensions of practical interest electrode lengths of the same order as the interelectrode spacings are desirable, (ii) moderately thick oxides enhance the tangential surface electric fields and increase the effectiveness of the channel-stop diffusion, (iii) lightly doped p-substrates are more resistant to the formation of electrostatic barriers in the gaps and yield faster devices because p-type conductivity silicon has a higher minority carrier mobility, and (iv) fixed charge at the Si-SiO_2 interface can have a significant influence on the device characteristics.

It is concluded that proper choice of both geometrical and electrical parameters is essential in obtaining optimum CCD performance; however, for such an optimized design, the transfer efficiency is for all practical purposes not limited by electrostatic considerations and is probably limited only by surface states. Theoretical limits of transfer efficiency based on these calculations are reported.

I. INTRODUCTION

With the invention[1] and initial investigation[2,3] of charge-coupled devices (CCDs), it became apparent that although conventional one-

dimensional considerations can lead to qualitative and heuristic arguments concerning the device operation, the phenomenon of charge coupling laterally along a semiconductor surface is essentially two-dimensional in nature and any quantitative understanding of the effect must begin with this premise. The purpose, therefore, of the present work is to use the solutions of the two-dimensional Poisson–Boltzmann equation obtained within the bounds of certain reasonable approximations to try to infer the basis of operation for the structures reported in the literature as well as to study new structures and predict their anticipated performance. Such inferences are obviously dependent upon a large number of considerations. For purposes of tractability, however, attention will be restricted to what is believed to be the key attributes of the device. Central to our considerations, therefore, will be the static surface potential and electric field profiles. These will be obtained through numerical iteration of the two-dimensional equations. In addition, the analysis is limited to the simple three-phase devices as originally described. The question of charge motion is then treated for the case of a sufficiently small charge density so that the fields are not appreciably altered by its presence. The equations of motion are then solved by an explicit quasi-static method. The usefulness and validity of such an artifical approach to the dynamic behavior of the device is discussed.

II. THEORETICAL MODEL

2.1 *General*

In Fig. 1, one unit cell of a three-phase CCD is illustrated in cross section (not to scale). For purposes of the model, the structure is assumed infinitely long in the direction normal to the page. Each electrode has a finite thickness t and length l and all are identical. They are spaced from each other by a distance g and from the semiconductor surface by the insulator thickness d. The interelectrode distance is taken as w $(= l + g)$ and the unit cell length as L $(= 3w)$. Although not shown in Fig. 1, in some calculations it will be assumed that the region between adjacent electrodes is occupied by a dielectric as may well be the case in an actual device manifestation. It is hypothesized that there exists an immobile charge of density Q_{ss} in the insulator in a small region adjacent to the insulator-silicon interface. The insulator is assumed to be silicon dioxide. The silicon is postulated as uniformly acceptor doped and sufficiently thick so that punch-through is not a consideration.

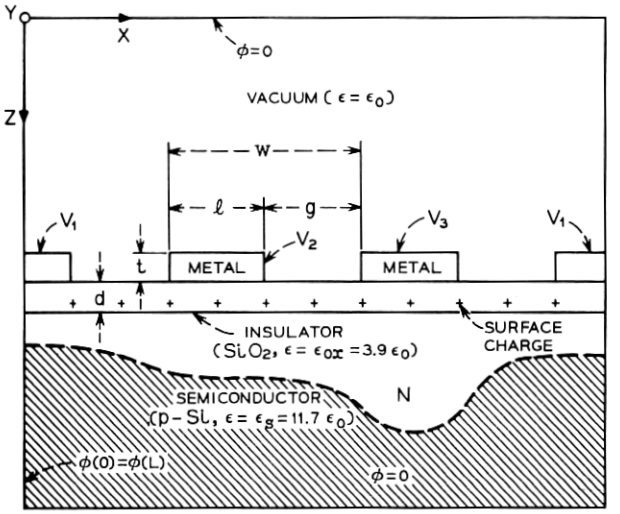

Fig. 1—Schematic cross section of a charge-coupled device unit cell showing the parameters and boundary conditions used in computer analysis.

Transfer of mobile charge at the interface by such a three-phase structure has been described qualitatively in the literature.[1-3] Briefly, electrons residing in an inversion layer are localized at the interface under the most positive electrode. This charge packet is moved to an adjacent area by increasing the potential of the neighboring electrode and decreasing the voltage on the initial electrode. Three electrodes per unit cell are required to insure directionality of charge transfer. Under ideal circumstances, the charge packet should move quickly, and in its entirety, from one area to the next when the proper voltages are applied to the electrodes. Assuming that the possibly important effects of trapping can be ignored, this charge motion is governed by the transport equation which in turn depends on the surface potential and electric field profiles. Our chief concern in the model, then, is to accurately obtain these profiles for specified electrode potentials and boundary conditions.

2.2 *The Dimensionless Poisson Equation*

The fundamental equation governing the electrostatic behavior in a semiconductor is, of course, the Poisson–Boltzmann equation

$$\nabla_x^2 \varphi = -\frac{\rho}{\epsilon} = \frac{q}{\epsilon_s}(N_A - N_D + n - p) : \text{semiconductor}, \qquad (1)$$

where N_A is the ionized acceptor concentration, N_D is the ionized donor density, and n and p are the electron and hole densities respectively. Similarly, in the oxide the appropriate equation is

$$\nabla_{\mathbf{x}}^2 \varphi = -\frac{Q_{ss}}{\epsilon_{ox}} \delta(x - x_s) : \text{insulator}, \tag{2}$$

where $\mathbf{x}_s$ is a vector defining the interface, and in the vacuum

$$\nabla_{\mathbf{x}}^2 \varphi = 0 : \text{vacuum}. \tag{3}$$

Equations (1) through (3) all possess the same form and, for purposes of generality and computational convenience, can be simultaneously recast into dimensionless form by use of new variables defined as

$$\begin{aligned} v &= \frac{\varphi}{V_o} \\ \boldsymbol{\alpha} &= \frac{\mathbf{x}}{x_o} \end{aligned} \tag{4}$$

where V_o and x_o are dimensioned constants arbitrarily chosen and usually assuming a value suggested by the problem parameters. The basic P–B equation then becomes

$$\nabla_{\boldsymbol{\alpha}}^2 v = -\frac{x_o^2}{V_o} \frac{\rho}{\epsilon} = -r(v, \boldsymbol{\alpha}). \tag{5}$$

In like manner, the dimensionless electric field is given by

$$\boldsymbol{\mathcal{E}} = -\nabla_{\boldsymbol{\alpha}} v \tag{6}$$

and is related to the true electric field by

$$\mathbf{E} = \frac{V_o}{x_o} \boldsymbol{\mathcal{E}}. \tag{7}$$

Note that the solution v is unchanged if $r(v, \boldsymbol{\alpha})$ is invariant to changes in x_o , V_o , and ρ. Assuming v to be available, the dimensional results can then be easily extracted by use of the scaling equations (4) and (7). To facilitate description of the physical operation of the device, the results in Section III are presented in dimensional form and the equations above can be easily applied to rescale to other dimensions or densities of interest.

2.3 *Approximations and Boundary Conditions*

In practice it is perhaps probable that, with the statement of boundary conditions, the problem can be solved by some numerical technique

without approximation. In the present problem such an approach is unnecessarily difficult and likely to be uneconomical as well.

In the normal operation of CCDs the potentials on *all* electrodes are kept sufficiently positive at all times to insure that the surface is maintained in a state of depletion (or inversion). Experimentally, it has been determined that this leads to the more efficient charge transfer because majority carriers cannot then reach the surface and be trapped to subsequently recombine with minority carriers in a passing inversion packet. In the analysis, this means that the depletion boundary never terminates at the surface and hence it may be justifiable to treat the majority carrier density in the P–B equation in a less than rigorous way. This observation leads to a significant reduction in computational labor. In the depleted (but not inverted) volume near the surface of a device with a p-type substrate, n, p, and N_D are much less than N_A and hence equation (1) reduces to a simple form of the Poisson equation. Conversely, deep in the bulk the hole density is large, although the electron density is still very small and $N_A - p \approx 0$. Consequently, equation (1) reduces to Laplace's equation if, as is commonly assumed, N_D is small. Within a few Debye lengths of the depletion boundary, however, the hole density is rapidly changing from near zero to N_A and cannot be ignored. However, as stated above, in a CCD the depletion boundary does not come close to the surface in normal operation and hence the precise manner in which the potential changes in the depletion boundary region is relatively uninteresting. Thus we assume that the hole density p is zero up to the depletion boundary and is equal to N_A beyond. This step function treatment of the majority carrier density is the essence of the "depletion edge" approximation and is expected to lead to accurate estimates of the true surface potential.

This method of treating the majority carrier density is the essential approximation of this work and with its statement the boundary conditions can now be specified:

(*i*) At a distance "far above" the device surface, the potential is uniform and equal to zero.

(*ii*) Each electrode is at a specified uniform potential (V_1, V_2, or V_3).

(*iii*) Deep within the bulk the potential is zero. The potential is never allowed to go negative in the semiconductor.

(*iv*) The potential is translationally periodic; i.e., $\varphi(o, z) = \varphi(L, z)$ where L is the unit cell length and z is the direction normal to the surface.

(v) At the vacuum-dielectric boundary and at the dielectric-semiconductor interface, the tangential component of the electric field and the normal component of the displacement field are conserved.

The numerical formulation of the problem and the relevant error considerations are treated in the Appendix.

III. RESULTS

3.1 *Static Surface Potential and Electric Field Profiles*

The surface potential, and consequently the electric field, throughout one bit of a CCD is a function of the semiconductor and oxide parameters, the geometrical configuration of the electrodes, and, of course, the impressed voltages. In this section the influence of each of these variables on the static surface potential and electric field is illustrated by several examples. For convenience these are presented in terms of specific dimensions as opposed to normalized coordinates. It is to be understood, however, that these results can be scaled to other dimensions by means of the equations of the previous section.

3.1.1 *Geometrical Influences*

Variation of the electrode length, the interelectrode spacing, and the oxide thickness has a significant effect on the surface potential profile and the relationship between these parameters must be considered carefully in predicting CCD behavior. The effect of modifying the electrode length is considered first. In Figs. 2a and b the surface potential and electric field are presented for electrode lengths of 3, 6, and 12 μm. For the other variables an oxide thickness of 3000 Å, a gap length of 3 μm, a doping density of 5×10^{14} cm^{-3}, and a positive oxide charge at the interface of 10^{11} cm^{-2} are assumed. At the instant of time in question, the electrode potentials are $V_1 = 0$, $V_2 = 4$ V, and $V_3 = 16$ V and it is assumed no minority carriers are present (the alternative case is considered separately in the next section). In this figure it is clear that the smaller electrode-length-to-gap-length ratio yields a larger tangential electric field under the center of the second electrode. A similar conclusion applies to the electric field under the first electrode. Elsewhere, the fields are very much alike. From the point of view of charge transfer, the tangential electric field under the second electrode is of particular interest. From Fig. 2b the minimum values of this field are about 40 V/cm, 500 V/cm, and 2000 V/cm for the 12-μm, 6-μm, and 3-μm electrode geometries respectively. For electrodes less than

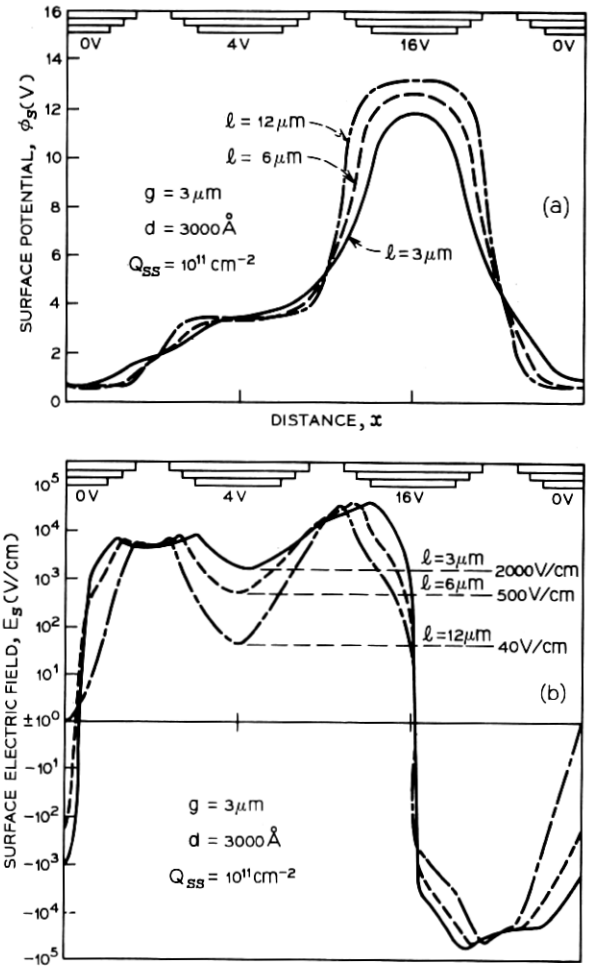

Fig. 2—Surface potential (a) and surface electric field (b) for three charge-coupled devices which differ in the electrode size but have the same gap length of 3 μm.

3 μm, the minimum field slowly continues to increase to about 10^4 V/cm; however, such electrode-length-to-gap-length ratios are not practical in terms of charge storage and efficient usage of silicon area. Moreover, for 2000 V/cm the region of nonlinear mobility is beginning and larger fields are of diminishing benefit.

Some effects of increasing the gaps can be inferred from the results of Fig. 2 and the scaling equations of the previous section without

additional computation. From equation (5), it follows from invariance of $r(v, \alpha)$ that as the dimensions are increased the voltage required to produce similar surface potential profiles increases quadratically. This will lead to similar performance since the surface electric field increases linearly if it is assumed that the mobility remains constant and the carrier drift velocity increases in proportion to the tangential field. Thus, direct scaling of the structures to larger dimensions rapidly results in inordinately large voltages. If the voltage is not increased, charge transfer may still occur but proceeds more slowly due to the decreasing fields and the increasing size of the unit cell. In addition, the surface potential in the large gap region becomes more dependent on the local charge density with the electrode voltages imparting a lesser influence. Thus, as will become clear in the next section, the control of such things as interface charge becomes more critical. For the case of constant voltages and constant unit cell length, the effect on the surface potential as the gaps are increased is shown in Fig. 3. Note the presence of an electrostatic barrier when the gap equals or exceeds 4 μm.

In a similar manner, it is expected that the electric fields will be altered by changing the oxide thickness. Using the same parameter values as in Fig. 2 for the structure with 3-μm electrodes, the surface electric field is shown in Fig. 4 for oxide thicknesses of 1500 Å, 3000 Å, and 5000 Å. For the 1500 Å oxide, the electric field dips to about 10^3 V/cm under the second electrode but peaks to almost 10^5 at the edge

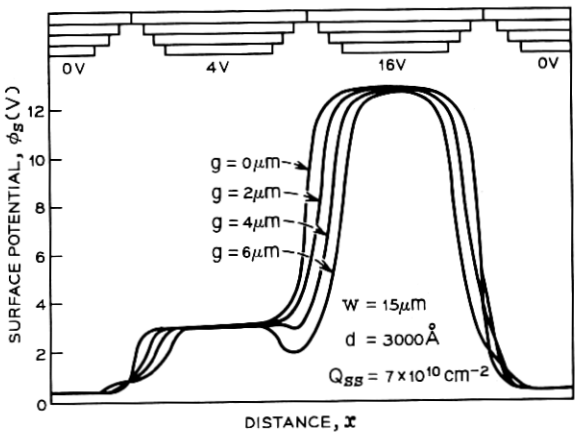

Fig. 3—The surface potential for charge-coupled devices with the same unit cell length but varying gaps and electrode sizes.

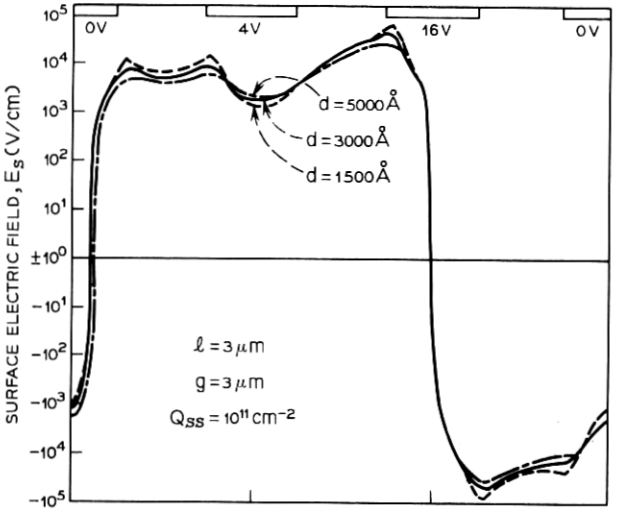

Fig. 4—Surface electric field for three charge-coupled devices which differ only in the oxide thickness.

of the third electrode. For the thicker oxides, the fields are more uniform with a minimum field of about 2×10^3 V/cm and a maximum of about 3×10^4 V/cm. For even thicker oxides, the tangential field begins to fall for a fixed set of gate voltages due to the rapidly decreasing surface potential. The better oxide thickness for this particular structure is approximately 3000 Å (or 0.1 of the electrode length) because it yields the greatest oxide capacitance per unit area (and hence charge handling capability) without sacrificing the magnitude of the electric field parallel to the surface. The above results imply that the moderately thick oxide enhances the ability of adjacent electrodes to couple effectively. In this context, two electrodes are said to be coupled when the tangential electric field at the surface is positive in the region between their centers. The larger the minimum field in this region, the more strongly the electrodes are said to be coupled.

The geometrical influences as presented in Figs. 2 and 4 indicate that in the range of practical interest (g = 1 to 10 μm), a preferred structure should possess an electrode-length-to-gap-length ratio of about unity and an oxide-thickness-to-electrode-length ratio of about 0.1, assuming all parameters are scaled appropriately. Furthermore, the smaller electrode lengths generally imply larger tangential fields, although the gains are probably marginal below 3 μm. These conclusions are in general consistent with intuitive notions about the effects of

capacitive fringing on which charge coupling is based. In an MOS capacitor, however, the magnitude of the fringing depends not only on the geometry but also on the charge density in the silicon and at the interface.

3.1.2 *Impurity Charge Density Influences*

In addition to the geometry of the device, the surface potential in a CCD is a function of the semiconductor impurity doping density and the (usually positive) ionic charge density at the interface. Ignoring for a moment the interface charge, the influence on the surface potential profile by modifying the substrate doping may be easily inferred from the scaling of equation (5). Thus, if the doping density is halved, the applied voltage may be also halved and a similar surface potential profile results in which the amplitude is reduced by a factor of two. Alternatively, the same voltages may be maintained but the structure enlarged by a factor of $\sqrt{2}$. In the former case the electric field also diminishes by a factor of two but the decrease in performance may be acceptable if the voltage is limited in the expected application. In the latter case the fields are undiminished but the increased bit length will proportionally reduce the charge transfer performance. Again, this may be acceptable if very fine features prove to be a difficulty. Unfortunately, in practice, materials more lightly doped than 5×10^{14} cm^{-3} are frequently nonuniform. Such nonuniformities could conceivably eliminate the anticipated benefits and result in a nonfunctioning device. Using more heavily doped material appears unprofitable unless one is capable of fabricating features smaller than 3 μm.

The influence of a charge density Q_{ss} at the interface is not so easily inferred. In Fig. 5a is plotted the surface potential for a CCD with 12-μm electrodes, 3-μm gaps, and differing Q_{ss} . The other parameters are the same as in Fig. 2. Note that for $Q_{ss} = 0$ there is a barrier-to-electron transfer in the gap between the second and third electrodes. As the magnitude of positive interface charge is increased, the barrier diminishes, eventually disappearing entirely. Thus, in an n-channel device, the normally occurring positive interface charge can be of substantial benefit. This is illustrated somewhat more dramatically in Fig. 5b. The parameters are as before except that the solid curve corresponds to a device with $Q_{ss} = 2 \times 10^{11}$ cm^{-2} and impressed voltages of 0, 4, and 16 volts. The dashed curve corresponds to a device with $Q_{ss} = 0$ and impressed voltages of 2.78, 6.78, and 18.78 volts. (The flatband voltage V_{FB} for 2×10^{11} cm^{-2} is 2.78 volts.) Quite clearly, the lack of Q_{ss} cannot be compensated for by adjusting the level of the

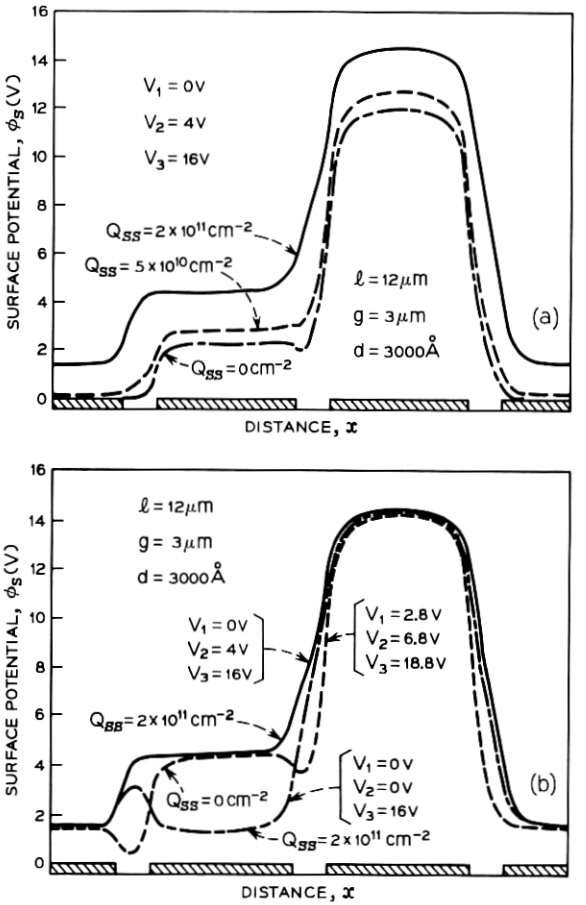

Fig. 5—Surface potential profiles for a 12-μm electrode charge-coupled device for differing values of interface charge and electrode voltage. (a) Electrode voltages held constant ($V_1 = 0$, $V_2 = 4$, $V_3 = 16$) but Q_{ss} varied. Note the "barrier" for $Q_{ss} = 0$. (b) The effect of interface charge on the surface potential. Solid line shows $\varphi_s(x)$ for $Q_{ss} = 2 \times 10^{11}$ cm^{-2}. Dashed curve shows $\varphi_s(x)$ for $Q_{ss} = 0$ and electrode voltages altered to compensate for flatband shift. Note the formation of large barriers in interelectrode gap. Dot-dash curve shows change of solid curve when second electrode is reduced to zero volts. Note the formation of a "pocket" in the gap between electrodes.

applied voltages without encountering large barriers to electron transport. Since the surface potential under the electrodes can be controlled by the applied voltage, the effect of this solid curve can be obtained by placing charge in the gaps only. However, there does not appear to be any advantage to this approach.

The presence of fixed charge at the interface can also cause some difficulties. The dot-dash curve in Fig. 5b illustrates the surface potential for a surface charge Q_{ss} of 2×10^{11} cm^{-2} and impressed voltages of 0, 0, and 16 volts. Note that in the gap between the first and second electrode there is a "pocket" in which electrons may be temporarily stored. Thus, for example, an electron briefly trapped in a surface state at the interface under the second electrode may, when emitted, proceed to the right or left. Those proceeding to the left are acquired by a trailing charge packet resulting in loss of transfer efficiency. This pocket may be eliminated by increasing the voltage on the first and second electrodes. The condition at which there is no pocket or barrier occurs when the gate voltage equals the surface potential. This can be easily calculated from the familiar equation relating the gate voltage to the surface potential

$$V_G - V_{FB} = \varphi_s + \alpha\varphi_s^{\frac{1}{2}} \tag{8}$$

where

$$\alpha = \frac{\sqrt{2\epsilon_s q N_A}}{C_o},$$

C_o = oxide capacitance.

If $V_G = \varphi_s$ it follows that when

$$V_1 = V_2 = V_G = \left(\frac{V_{FB}}{\alpha}\right)^2 \tag{9}$$

the surface potential is "level" and no barrier or pocket exists in the gap between the first and second electrode. Conversely, difficulties with small pockets may be avoided by allowing V_2 to return to its minimum potential slowly enough so that the charge has the maximum opportunity to proceed to the right. For larger pockets such an approach may not be adequate. Both pockets and barriers become larger for greater interelectrode spacing.

In addition to adjusting the doping, the electrode length, and the oxide thickness, the strength of coupling may be influenced by including a dielectric in the interelectrode spacing. If the surface potential and electric field for the 12-μm electrode, 3-μm gap configuration discussed in Fig. 5 is recalculated for the case when Q_{ss} is set equal to zero, the solid curves of Figs. 6a and b result. Adding insulating material in the gaps with the same dielectric constant as SiO_2 but changing nothing else yields the dotted curves. Although the barrier has not

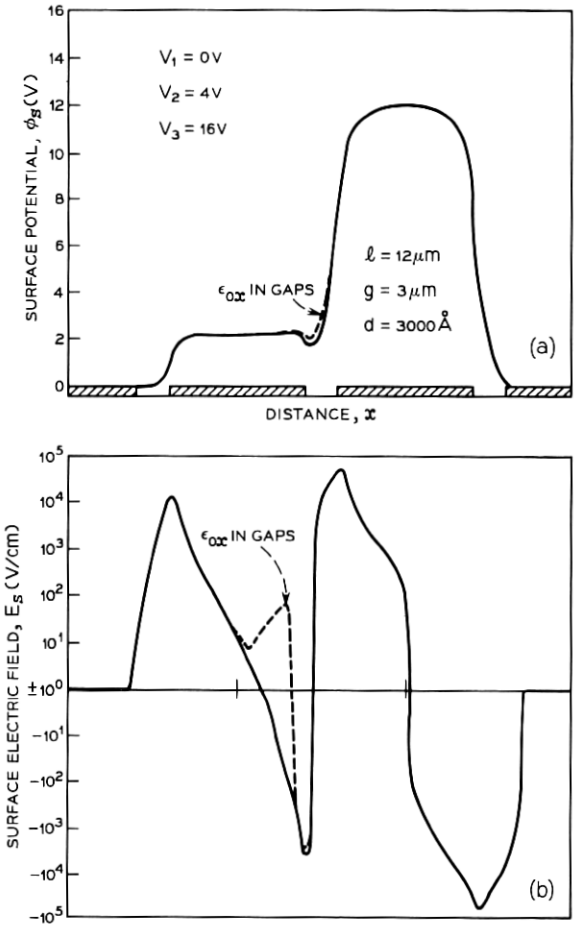

Fig. 6—Surface potential (a) and surface electric field (b) for two charge-coupled devices differing only in the presence of the dielectric in the region between electrodes.

vanished, it has definitely decreased and the fields indicate a more favorable coupling posture. In these calculations the electrode thickness is assumed to be 2000 Å and the observed results are believed attributable to more effective coupling of the electrode edges to the silicon surface. A material in the gaps with a higher dielectric constant would be even more effective in reducing or perhaps eliminating the barrier.

Before proceeding to the discussion of minority carrier transport in these structures, the surface potential in the direction normal to the channel is treated so that the effects of the channel-stop diffusion

may be considered. The appropriate model geometry is shown in Fig. 7a. The p^+ channel-stop diffusion is hypothesized 2 μm deep with an abrupt junction. Assuming a substrate doping of 5×10^{14} cm^{-3}, a channel-stop diffusion of 10^{18} cm^{-3}, and a gate voltage of 25 V, the surface potential and electric field shown in Fig. 7b and 7c result for oxide thicknesses of 2000 Å and 3000 Å. Note that near the channel-stop diffusion the maximum electric field approaches the breakdown field for silicon in both cases. Avalanche breakdown at the channel edges gives rise to unwanted currents thereby degrading device performance. In seeking methods to reduce the peak electric field it was observed that field profiles are relatively insensitive to parameter changes, with the exception of substrate doping and, of course, the applied voltage. Increasing the oxide thickness helps to the extent of reducing the surface potential for a given gate voltage and, therefore, has only a small effect on the maximum field as illustrated in Fig. 7c. The reduced potential, however, keeps the surface in the channel-stop region well below threshold thereby preventing large quantities of spurious dark current from coupling with the active region. Changing the doping of the channel-stop diffusion has only a very small effect on the maximum field, since by its very nature this diffusion must effectively hold the surface potential to small values in this region. It is concluded, then, that avalanching can most easily be avoided by limiting the voltage operation to values less than about 25 V, although an increase in the substrate doping density from 5×10^{14} cm^{-3} to larger values is also a possibility.

3.2 *Charge Transport*

When the surface potential and electric field profiles in a CCD are like those shown, for example, in Fig. 2, any electrons (minority carriers) under the second electrode will be rapidly transferred to the region under the third electrode. In this section we discuss the time behavior of this charge transfer and attempt to infer its dependence on surface potential, surface electric field, and minority carrier charge density.

3.2.1 *Analytic Transport Equation*

Before launching into a presentation of the computer predictions for the time dependence of charge transfer, it is useful to investigate the nature of the transport phenomenon by analytically studying the relevant equations. From such an analysis we can glean basic functional forms which shall prove useful in the interpretation of the computer results.

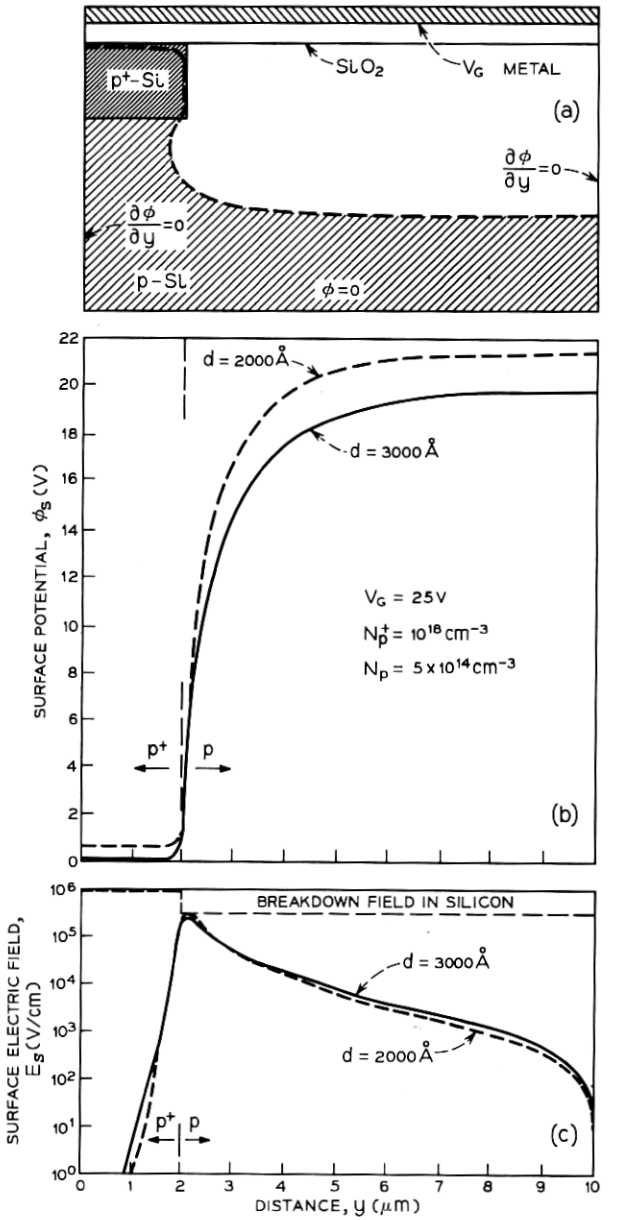

Fig. 7—Cross section (a) of charge-coupled device electrode normal to the channel direction showing channel-stop diffusion as used in computer analysis. Surface potential (b) and surface electric field (c) across channel-stop boundary for fixed electrode voltage and two oxide thicknesses.

In one dimension, the equation for current flow in a semiconductor is well known to be

$$j = \mu(E)\left(\rho E - \frac{kT}{q}\frac{\partial \rho}{\partial x}\right) \tag{10}$$

where $\mu(E)$ is the mobility, E is the surface electric field, and ρ is the minority carrier charge density. It is convenient to divide the surface electric field into two contributions

$$E = E_\rho + E_s$$

where E_s is the electric field arising from the device geometry as described earlier and E_ρ is the field contribution resulting from variations in the charge density of minority carriers. This latter contribution is easy to derive for the case of a large MIS capacitor. From equation (8), it follows almost immediately that the inversion charge density is given by

$$\rho = C_o(V - \varphi_s) - \sqrt{2qN\epsilon_s}\,\varphi_s^{\frac{1}{2}} \tag{11}$$

where $V = V_G - V_{FB}$. Differentiating (11) with respect to x results in

$$\frac{\partial \rho}{\partial x} = -\left(C_o + \sqrt{\frac{qN\epsilon_s}{2\varphi_s}}\right)\frac{\partial \varphi_s}{\partial x}$$

$$= -(C_o + C_d)E_\rho$$

or

$$E_\rho = -\frac{1}{C_o + C_d}\frac{\partial \rho}{\partial x} \tag{12}$$

in which C_d is the depletion capacitance.

The thermal contribution in equation (10) may also be treated in terms of an effective field if it is divided by the charge density.

$$E_{\text{th}} = -\frac{kT}{q}\frac{1}{\rho}\frac{\partial \rho}{\partial x} = -\frac{kT}{q}\frac{\partial(\ln \rho)}{\partial x}. \tag{13}$$

In many instances the "thermal" field is small, initially, in comparison to E_ρ and E_s but can be important in determining the asymptotic behavior of the charge decay.

It is now possible to identify three physical cases as suggested by the form of equation (10). These occur when E_s is small and the electric field E is dominated by E_ρ, when E_s dominates and E_ρ is small, and when E_ρ and E_s are comparable. In each case E_{th} is assumed to be

small initially compared to the dominant field. In any of these cases it is possible to eliminate the current dependence by use of the continuity equation

$$\frac{\partial \rho}{\partial t} + \frac{\partial j}{\partial x} = 0. \tag{14}$$

The analytic transport equation is then

$$\frac{\partial \rho}{\partial t} = -\frac{\partial}{\partial x}\left\{\mu(E)\left[\rho E_s - \left(\frac{\rho}{C_o + C_d} + \frac{kT}{q}\right)\frac{\partial \rho}{\partial x}\right]\right\}. \tag{15}$$

In the case when the tangential fields resulting from geometrical factors are small ($E_\rho + E_{\text{th}} \gg E_s$), equation (15) reduces to a form of the diffusion equation

$$\frac{\partial \rho}{\partial t} = \frac{\partial}{\partial x}\left\{\left[\mu\left(\frac{\rho}{C_o + C_d} + \frac{kT}{q}\right)\right]\frac{\partial \rho}{\partial x}\right\}. \tag{16}$$

If the temperature-dependent term is negligible and μ and C_d are assumed constant, the variables easily separate* and the normalized time-dependent part, which we shall designate $\epsilon'(t)$, has the form

$$\epsilon'(t) = \frac{t_0}{t + t_o} \tag{17}$$

where t_o is a constant of integration determined by the boundary conditions.[4] Note that in this case $\epsilon'(t)$ goes to zero very slowly in time thereby implying that the transfer efficiency will suffer at high frequencies. However, when ρ becomes sufficiently small, the temperature-dependent term can no longer be ignored. In the limit when the thermal term dominates, equation (16) assumes the standard Fick's equation form. Following R. J. Strain and N. L. Schryer,[5] the gradient of the charge density may be assumed to be zero under the left edge of the electrode where the charge is initially located (charge transfers to the right). The solution is then an infinite series of the form

$$\rho = \sum_{n=1}^{\infty} a_n \exp\left\{-\left[\frac{(2n-1)\pi}{2(w + x_o')}\right]^2 Dt\right\} \cos\left[\frac{(2n-1)\pi}{2}\frac{x'}{w + x_o'}\right] \tag{18}$$

where D is the diffusion coefficient ($= \mu\, kT/q$), x' is a new spatial variable with its origin at the left edge of the electrode, and x_o' is a constant determined by the boundary condition at $x' = L$. When the carriers reach $x' = L$, they move off at a constant velocity v_L deter-

* In this and the ensuing cases it is assumed that separable boundary conditions are applicable.

mined by the electric field E_L present at this edge (and in the inter-electrode gap region) through the relation $v_L = \mu E_L$. Thus the appropriate boundary condition is

$$\frac{j(x' = L)}{\rho(x' = L)} = -D \frac{\partial \ln \rho}{\partial x'}\bigg|_{x'=L} = v_L .$$

For nominal values of v_L , x'_o is much less than w and may be assumed negligible corresponding to the case $v_L = \infty$. The coefficients a_n are determined by the initial condition for the charge density distribution. If the distribution is such that it is rich in harmonics, the time decay of the charge density for small t is a large summation of exponentials not unlike an error function. After a sufficiently long time, however, the leading term will dominate and the decay will be purely exponential with the charge density distribution assuming a cosine form.

In the other extreme, when ρ is large, changes in C_d may not be ignorable because in this case the depletion region is almost totally collapsed. Hence, for a very short time interval near zero, $\epsilon'(t)$ will deviate from (17) but the intermediate and long-time behavior are unaffected. Thus, in the case when $E_\rho + E_{\text{th}} \gg E_s$, the charge density under an electrode decays in approximately a hyperbolic fashion initially and exponentially asymptotically.

In the case when the geometrically induced fields are large compared to the charge induced fields ($E_s \gg E_\rho + E_{\text{th}}$), equation (15) reduces to the field-aided form

$$\frac{\partial \rho}{\partial t} = -\frac{\partial}{\partial x}[\mu \rho E_s]. \tag{19}$$

As above, the variables separate and the normalized time-dependent part has the form

$$\epsilon'(t) = \exp\left\{-b\left(\frac{\mu E_s}{w}\right)t\right\} \tag{20}$$

where b is a constant of integration and it has been assumed that μ and E_s are constant. Note that in this case the form of the charge decay is similar to the asymptotic form of the previous case. It is clear, however, that (20) will approach zero more rapidly than (18) when

$$E_s > \frac{kT}{wq} \tag{21}$$

if we make the reasonable assumption that the constant b is comparable to $(\pi/2)^2$. If the electrode spacing w is taken to be 10 μm, inequality (21) becomes

$$E_s > 26 \text{ V/cm.} \tag{22}$$

This condition can be easily achieved by designing the CCD structure according to the geometrical considerations outlined earlier.

Finally, in the case when E_p and E_s are comparable, equation (15) does not simplify and the variables are not separable. Thus we can say nothing quantitative. Qualitatively, however, it is expected that $\epsilon'(t)$ in this case would be an admixture of the above results with an approximate hyperbolic-exponential form.

3.2.2 *Computer Analysis of Charge Transport*

A numerical approach to the question of charge transport in a CCD may proceed in one of two ways. Perhaps the most obvious is to return to equation (15) and solve it numerically using a standard technique for dealing with partial differential equations (such as the Crank–Nicholson scheme) subject to some reasonable boundary conditions. The required electric field profile is either given some approximate mathematical form or taken digitally from the results of Section 3.1. Alternatively, one may return to the current equation (10) and recast it in the form of an effective carrier velocity for each point along the surface. Then proceeding sequentially in time, the trajectory of each carrier is computed for a small time increment Δt during which the velocity is assumed constant. After Δt, a new velocity is computed for each carrier resulting in a new trajectory and so on. At time zero, all carriers are under electrode #2 and the time-dependent transfer inefficiency $\epsilon(t)$ is taken to be the number of carriers *not* under electrode #3 divided by the total number of carriers as a function of time. The transfer inefficiency $\epsilon(t)$ is analogous to the time-dependent solution $\epsilon'(t)$ discussed in the previous section but without the spatial dependence separated out.

Clearly, the latter approach, although conceptually more straightforward, is economical only for a relatively small number of minority carriers. This, however, is just the case we wish to examine. In order to treat the case of large carrier densities, it is necessary to include these carriers explicitly in the solution of the Poisson equation. Whereas this in itself is not difficult, it is necessary to recompute the solution at *every* time step. It is possible that the cost of such an analysis would not be prohibitively large; nonetheless, it is essential to ask what additional knowledge is obtained. Reflection on the discussion in the previous paragraph reveals that the only significant addition is the very short time behavior when electrostatic repulsive forces between

carriers are large. The transfer inefficiency function then falls quickly under a combined form of the exponential and hyperbolic behavior discussed earlier. This mode of behavior, however, lasts for a time very short compared to the asymptotic behavior, which has the principle influence in determining how much charge is left behind in a practical device application.

Based on these considerations much can be learned by investigating only small charge densities. This is done by means of the effective velocity approach and using nearest and next nearest neighbors to estimate local charge density. Thus, from (10), the distance Δx traveled by an electron in time Δt is

$$\Delta x \cong \mu(E)\left(E(x) - \frac{kT}{q}\frac{\partial \ln \rho}{\partial x}\right)\Delta t. \tag{23}$$

For the field-dependent mobility the empirical relation

$$\mu(E) \approx \frac{\mu_0 v_s}{\mu_o \left| E - \frac{kT}{q}\frac{\partial \ln \rho}{\partial x} \right| + v_s} \tag{24}$$

is used where v_s is the scattering limited velocity of the electrons in silicon and μ_o is the low field mobility. Using time increments of 0.002 ns and charge densities of a few times 10^9 cm^{-2} the charge motion is computed for the first nanosecond for each of the structures described by the results of Fig. 2. The time-dependent transfer inefficiency for each of these is plotted in Fig. 8. Note that in each trace the inefficiency initially stays at unity for 0.15 to 0.30 ns, during which time the first carriers move across the interelectrode gap. This is followed by a rapid fall, corresponding to the hyperbolic behavior indicated earlier, after which the decay lapses into an exponential. For each curve an exponential is matched to the appropriate data. The resulting time constants are

$$\tau = \begin{array}{l} 0.08 \text{ ns: } 3\text{-}\mu\text{m electrodes} \\ 0.5 \text{ ns: } 6\text{-}\mu\text{m electrodes} \\ 3.6 \text{ ns: } 12\text{-}\mu\text{m electrodes.} \end{array} \tag{25}$$

Note that if these time constants are used in equation (20) to calculate the electric field modified by the undetermined constant, bE_s, quantities are obtained which are consistent with the average fields in the transfer region as inferred from Fig. 2b if $b \approx 1$.

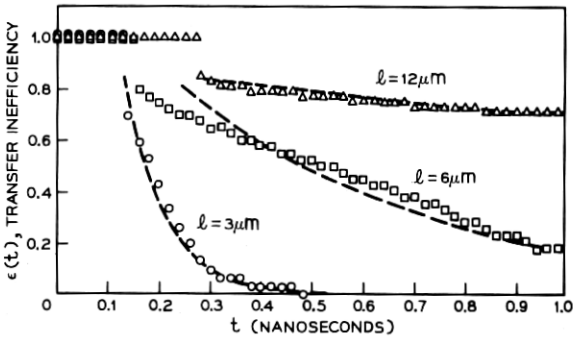

Fig. 8—Time-dependent transfer inefficiency for the same charge-coupled devices as in Fig. 2.

$$bE_s \approx \begin{cases} 10^4 \text{ V/cm: 3-}\mu\text{m electrodes} \\ 3 \times 10^3 \text{ V/cm: 6-}\mu\text{m electrodes} \\ 7 \times 10^2 \text{ V/cm: 12-}\mu\text{m electrodes.} \end{cases}$$

Thus, for times large compared to the characteristic time constant, equation (20) with $b = 1$ is useful in estimating transfer inefficiency if the average field is available. Based on such an exponential form, the transfer efficiency $\eta(= 1 - \epsilon)$ after N unit cells can be expressed

$$\eta(t) = (1 - \epsilon(t))^{3N} \tag{26}$$

where

$$\epsilon(t) = e^{-t/t_o}.$$

If ϵ is assumed small compared to unity, equation (26) becomes

$$\eta(t) \approx e^{-3N\epsilon} \approx 1 - 3N\epsilon \tag{27}$$

where the first approximation is valid if $3N\epsilon^2 \ll 1$ and the second is valid if $3N\epsilon \ll 1$. The appropriate time t used depends on the frequency of operation and t_o depends on the average electric field as described above. It is clear from (27) and previous discussion that an extremely high transfer efficiency is obtainable in principle in a properly designed charge-coupled device.

IV. CONCLUSIONS

The choice of geometrical and electric factors in the construction of a charge-coupled device influence the charge transfer performance of such structures. In particular, the following points are evident.

(*i*) For dimensions of practical interest (1–10 μm) electrode lengths comparable to interelectrode spacings are desirable.

(*ii*) Generally, moderately thick oxides (~3000 Å) enhance the tangential surface electric fields as well as increase the efficacy of the channel-stop diffusion without a serious loss in charge handling capability.

(*iii*) The presence of a dielectric in the interelectrode gaps enhances the coupling strength of adjacent electrodes. A slightly conductive material (a so-called resistive sea) which allows charge to move between electrodes over the oxide surface in the gap region can be made to accomplish the same objective.

(*iv*) Uniform, lightly doped substrates are generally more resistant to the formation of electrostatic barriers in the gaps than more heavily doped material.

(*v*) A p-type conductivity silicon substrate is preferable to n-type material because of the increased mobility and the favorable influence of the normally occurring positive surface charge, although at the anticipated performance levels suitable p-channel devices can be made if these restrictions are taken into consideration.

(*vi*) There is an optimum surface charge density depending on the oxide thickness and substrate doping density.

(*vii*) For a CCD which is nearly optimized with respect to the considerations discussed in this paper, the transfer efficiency is for all practical purposes not limited by electrostatic considerations.

Remaining to be investigated are the proposed two (or four) phase structures which call for either two levels of metallization or the addition of surface charge near the interface.[6] Furthermore, the effect of surface states on transfer efficiency has been completely ignored and for an appropriately designed CCD will likely represent the limiting factor. With the exposition of the basic electrostatic considerations described in the present work, these important questions can now be investigated on a solid physical foundation and future CCDs can be designed confidently.

APPENDIX

Numerical Formulation

Except for cases of simple geometry, the Poisson equation cannot be solved analytically and the use of numerical methods is necessary. As a result of the great interest in elliptic equations and in the Poisson

equation in particular, a number of satisfactory numerical techniques exist for finding the solution within a bounded region Ω with perimeter Γ on which the solution is specifiable.

The region Ω and the boundary conditions on Γ usually suggest themselves by considerations of symmetry. These were discussed earlier for the problem of a three-phase charge-coupled device and are illustrated in Fig. 1. The geometry of the region is seen to be a simple rectangle characterized by linear interface boundaries. In such cases, an explicit, finite difference method employing successive overrelaxation (SOR) is often satisfactory.[7] While more elegant methods such as the implicit or finite element techniques are equally valid, adequate accuracy and economy is possible with the simple SOR approach. With more exotic geometrical configurations or boundary conditions, the alternative methods may be more advantageous.

The region Ω is segmented into $p \times q$ rectangular cells and each node is labelled (i, j). Each rectangular cell is not necessarily the same size and the length of the sides are given as h_i and k_j . In this notation the potential at any mesh point is estimated by

$$\varphi^e_{i,j} = M^2\left\{\frac{h_{i-1}\varphi_{i+1,j} + h_i\varphi_{i-1,j}}{h_i h_{i-1}(h_i + h_{i-1})} + \frac{k_{j-1}\varphi_{i,j+1} + k_j\varphi_{i,j-1}}{k_j k_{j-1}(k_j + k_{j-1})}\right\} + \frac{\rho_{i,j}}{2\epsilon_{i,j}} \tag{28}$$

where

$$M^2 = \frac{h_i h_{i-1} k_j k_{j-1}}{h_i h_{i-1} + k_j k_{j-1}},$$

$\rho_{i,j}$ is the charge density, and only nearest neighbors have been used in estimating the derivatives (the so-called five point approximation). To compute the solution, the potential is successively calculated using (28) for each node in the field. After completing a step through the field, the process is continued repeatedly until by some means (discussed below) it is determined that the result is within a certain specified precision of the solution and the iteration process is ended. The solution is often approached more rapidly if, instead of (28) above, the potential at each node point is estimated by a linear combination of (28) with the previous estimate. Thus, after n iterations of the region Ω, the potential at any node is given by

$$\varphi^{(n)}_{i,j} = (1 - \alpha)\varphi^{(n-1)}_{i,j} + \alpha\varphi^e_{i,j} \tag{29}$$

where α is the relaxation factor and determines the rate of convergence. For any given problem there exists an α for which the rate of convergence is maximized provided the sequence in which the nodes are calculated possesses a consistent ordering designated "Property A."[4] If α is less than unity, the convergence is "underrelaxed"; and if α is greater than unity, the convergence is "overrelaxed." In practice the maximum rate of stable convergence is usually obtained when $\alpha > 1$ and hence the name successive-overrelaxation.

A detailed description of consistent orderings of the nodes possessing Property A is available in the literature. In the present work the common "checkerboard" array has been used. The nodes of region Ω are divided into two groups, A and B, and each iteration is composed of a step through the A group followed by a step through the B group. All the nodes in Ω are categorized into A or B in a manner exactly analogous to the familiar black and white squares of the chessboard. Note that when computing the potential at a node point in group A, only the potentials at node points of group B are used. All consistently ordered sequences possess this property.

When the region Ω is rectangular and the calculation sequence is consistently ordered, it is possible to analytically determine the optimum relaxation factor. It is given by the expression

$$\alpha_{\text{opt}} = 2\left(1 - \frac{\pi}{pq}\sqrt{\frac{p^2 + q^2}{2}}\right). \tag{30}$$

When Ω is not rectangular or circular, the optimum relaxation factor cannot be computed in closed form and methods exist for estimating it numerically.[6] As a result of the unusual boundary condition for the depletion edge, the region in the present problem is not truly rectangular. Nonetheless, the relaxation factor calculated on the basis of (30) is almost identical to the value estimated numerically, so long as the bottom of the rectangle is within a few mesh points of the lowest part of the depletion edge. This is fortuitous because, in general, the depletion boundary changes with every problem and recomputation of α_{opt} each time would be prohibitive.

Finally, it is possible to estimate the error of the numerical solution. Actually, there are two kinds of error to consider. One arises from the quantization of the space and the replacement of the differential equation by a finite difference equation. The other kind of error arises from the termination of the calculation after a finite number of iterations. The former is of order μ^2, where μ^2 is the dimensionless equivalent of M^2 defined in equation (28) and obtained by scaling the area of Ω to unity.

The quantization error is typically not a problem and can usually be made acceptably small without using a prohibitively large number of mesh sites. It is to be noted that, whereas the quantization error in the potential is $O(\mu^2)$, the error in the electric field is $O(\mu)$.

Truncation error can also be estimated. After many iterations (the exact number depending on the specific problem) the ratio of the errors e^n from one iteration to the next approaches a constant λ at any given mesh point

$$\frac{|e^{n+1}|}{|e^n|} \approx \lambda. \tag{31}$$

The constant λ is in turn related to the "residuals" d^n

$$\lambda^2 \approx \frac{d^{n+1}}{d^n} \tag{32}$$

where a residual is defined

$$d^n = \left[\frac{1}{pq}\sum_{i,j}^{p,q} (v_{i,j}^{(n)} - v_{i,j}^{(n-1)})^2\right]^{\frac{1}{2}}$$

and $v_{i,j}^{(n)}$ is the normalized potential [equation (4)]. Thus, in the iteration region where the convergence is monotonic the mean error after n iterations is given as

$$\langle e^n \rangle = \sqrt{d^n}. \tag{33}$$

In the CCD problem discussed in the text, the region Ω is divided into approximately 50×90 cells. In the direction parallel to the semiconductor surface, the nodes are equally spaced. In the direction normal to surface, the spacing is 500 Å in the vicinity of the interface but increases linearly deep into the bulk and quadratically into the vacuum. In this way the voltage change from one node to the next is always about the same. Such an approach yields the greatest economy with no real loss in accuracy. Based on (33), a mean error in the potential of less than 10^{-2} is typically obtained after less than 10^2 iterations. The constant λ defined in (31) generally is established after about 20–30 iterations. In any practical problem this represents a lower limit to the required number of iterations. Once λ is known, the number of additional iterations needed to reduce the error to an acceptable value can be determined.

REFERENCES

1. Boyle, W. S., and Smith, G. E., "Charge Coupled Semiconductor Devices," B.S.T.J., *49*, No. 4 (April 1970), pp. 587–593.

2. Amelio, G. F., Tompsett, M. F., and Smith, G. E., "Experimental Verification of the Charge Coupled Device Concept," B.S.T.J., *49*, No. 4 (April 1970), pp. 593–600.
3. Tompsett, M. F., Amelio, G. F., and Smith, G. E., "Charge Coupled 8-Bit Shift Register," Appl. Phys. Ltrs., *17*, 1970, pp. 111–115.
4. Engler, W. E., Tiemann, J. S., and Baertsch, R. D., "Surface Charge Transport in Silicon," Appl. Phys. Ltrs., *17*, 1970, p. 469.
5. Strain, R. J., and Schryer, N. L., unpublished work.
6. Krambeck, R. H., Walden, R. H., and Pickar, K. A., "Implanted Barrier Two-Phase Charge-Coupled Device," Appl. Phys. Ltrs. *19*, 1971, pp. 520–522.
7. Smith, G. D., *Numerical Solution of Partial Differential Equations*, New York: Oxford Univ. Press, 1965.